

# Reconstruction of Low-Speed Crashes using the Quasi-Static Force vs. Deformation Characteristics of the Bumpers Involved in the Crashes

William Scott, Enrique Bonugli, Herbert Guzman and Daniel Swartzendruber  
Biodynamic Research Corporation

## ABSTRACT

The purpose of this study was to determine if quasi-static (QS) bumper force-deformation (F-D) data could be used in a low-speed bumper-to-bumper simulation model (1) in order to reconstruct low-speed crashes. In the simulation model, the bumpers that make contact in a crash are treated as a system. A bumper system is defined as the two bumpers that interact in a crash positioned in their orientation at the time of the crash. A device was built that quasi-statically crushes the bumpers of a bumper system into each other and measures the compression force and the deformation of the bumper system. Three bumper systems were evaluated. Two QS F-D measurements were performed for each bumper system in order to demonstrate the repeatability of the QS F-D measurement. These measurements had a compression phase and a rebound phase. A series of crash tests were performed using each bumper system. In each crash test, a stationary target vehicle was struck on the rear bumper by the front bumper of a bullet vehicle. Both vehicles were instrumented with accelerometers. The bullet vehicle had load cells at the front that measured crash forces and a displacement sensor that measured the deformation of the bumper system during the crash. The crash tests were performed over a range of impact speeds for the bullet vehicle. The compression QS F-D data were used as an input to the simulation model in order to reconstruct the vehicle motions in the crash tests. The other inputs required to simulate a crash test were the impact speed of the bullet vehicle, the vehicle masses and the coefficient of restitution measured in the crash test. The study demonstrated that the simulation model with the QS F-D data accurately recreated the velocities of the target and bullet vehicle in the crash tests.

**CITATION:** Scott, W., Bonugli, E., Guzman, H. and Swartzendruber, D., "Reconstruction of Low-Speed Crashes using the Quasi-Static Force vs. Deformation Characteristics of the Bumpers Involved in the Crashes," *SAE Int. J. Passeng. Cars - Mech. Syst.* 5(1):2012, doi:10.4271/2012-01-0598.

## INTRODUCTION

Quantifying the severity of low-speed bumper-to-bumper crashes has always been a challenge because most of the classical crash reconstruction techniques are intended to be used in crashes that produce significant amounts of crush (2). In a low-speed bumper-to-bumper crash, where injuries are alleged to have occurred, there may be no measureable crush or limited areas of focal damage that are difficult to quantify. In many cases the only source of information about the damage to each vehicle are photographs of the vehicles and repair estimates.

Thus far there have been two main approaches to modeling a low-speed crash. The first approach is to treat the vehicles as rigid structures, model the bumpers as spring/dashpot systems and then solve the governing differential equations with the appropriate initial conditions (3,4,5,6).

The inputs required by a spring/dashpot model to simulate a specific crash are the stiffness and damping coefficients for the bumpers that interact in the crash. These coefficients are generally not known. The accuracy of the simulation relative to the crash being analyzed cannot be determined as there is no way to correlate the simulation damage with the damage pattern of the bumpers in the actual crash. The second approach, the Momentum-Energy-Restitution (MER) method, is based on rigid body impact mechanics and uses impulse, conservation of momentum, conservation of energy and restitution to determine the change in velocity ( $\Delta V$ ) of the vehicles in the crash (7,8,9). In order to estimate the  $\Delta V$  for a vehicle in a specific crash the MER method requires a value for the coefficient of restitution ( $\epsilon$ ) and an estimate of the energy absorbed by each vehicle during the crash. While there are methods to estimate  $\epsilon$  for a given crash situation, it is difficult to determine the amount of energy absorbed by

both vehicles during the crash, especially if the damage to each bumper is minimal and non-uniform.

Previously, a simulation model was developed to recreate low-speed bumper-to-bumper crashes where the only damage was to the bumpers (1). The impact force used in this simulation model is directly related to the force-deformation (F-D) characteristics of the bumpers involved in the crash being investigated. The model treats the bumpers that contact in a crash as a system, which is defined as the two bumpers that interact in a crash orientated as they were at the time of contact. Previously, dynamic F-D data measured in crash tests were used as input to the simulation model in order to recreate the vehicle dynamics in those crash tests (1). In a real world crash investigation the input to the model is intended to be the quasi-static (QS) force-deformation (F-D) characteristics of the bumper system and, therefore, a basic assumption of this simulation technique is that the QS F-D characteristics of the bumper system can represent the dynamic F-D characteristics in a low-speed impact. The QS F-D measurement is also intended to create damage patterns to the bumpers that are similar to or greater than the damage to the bumpers in the crash being investigated. A comparison of the damage obtained in the QS F-D measurement with the damage to the bumpers in the crash being investigated provides a metric to determine how well the impact forces in the simulation represent the impact forces in the actual crash.

The goal of the present study was to determine if the QS F-D characteristics of a bumper system can be used to reconstruct a low-speed crash with the simulation model. Three bumper systems were evaluated. The first step in this study was the measurement of the QS F-D characteristics of each bumper system. Next, a series of crash tests were performed using each bumper system. The crash tests were performed for two reasons. First, they provided data on the dynamic F-D characteristics of the bumpers. Second, the crash tests provided a known event that the simulation model and the QS F-D data could be used to reconstruct. In each crash test the dynamic F-D characteristics of the bumper system were measured and compared with the QS F-D characteristics. The QS F-D data were used as input data in the simulation model along with the test vehicle masses, and the closing velocity and the coefficient of restitution measured in the crash test. The simulation model was then used to calculate the vehicle dynamics in the crash test. Finally, the simulated vehicle dynamics were compared with the vehicle dynamics measured in the crash tests in order to validate the effectiveness of this reconstruction technique.

## METHOD

### QUASI-STATIC FORCE-DEFORMATION MEASUREMENTS

In this study three bumper systems were evaluated, each of which was composed of the rear bumper of the struck vehicle, the target vehicle, and the front bumper of the

striking vehicle, the bullet vehicle. The bumpers were from passenger cars, a van and SUVs. The lateral positions were set so that the centers of the bumpers were in line. The vertical orientations of the bumpers in each system were determined by performing exemplar vehicle match-ups. The same bumper orientations were used in all of the QS F-D measurements and crash tests for a given bumper system. Table 1 details the origins of the bumpers in each bumper system, which are called Bumper System A, B and C.

**Table 1. Target and bullet vehicle bumpers used in each test series.**

Bumper System	Target Vehicle Bumper - Rear Bumper	Bullet Vehicle Bumper - Front Bumper
A	1994 Toyota Tercel	2003 Chevy Express Van
B	2002 Honda Civic	2007 Ford Escape
C	2008 Honda Civic	2005 Kia Sedona

Previous research indicated that the geometry of the surface that applies the force affects the QS F-D characteristics of an individual bumper (1), thus the best way to replicate the physical characteristics of the other bumper in the QS F-D measurement is to use that bumper. Therefore the QS F-D data for a bumper system were obtained by pushing the two bumpers of a bumper system into each other. In order to perform the QS F-D measurement a device was built that quasi-statically crushes the two bumpers into each other while they are in the proper relative orientation and measures the compression force and the deformation of the bumper system. Figure 1 shows a photograph of the device, which is colloquially called the bumper crusher. The QS F-D data of each bumper system were measured twice in order to determine how repeatable the measurement was.

The bumper crusher consists of a fixed plate to which one bumper is attached and a moveable plate to which the other bumper is attached. The moveable plate is pushed along a track by two hydraulic cylinders. A load cell (1210-A0 25, Interface, Inc) attaches each hydraulic cylinder to the plate, and measures the force applied to the moveable plate by that piston. Two displacement transducers, a string pot (PT101, Celesco, Inc.) and a LVDT (E-Series, Temposonics, MTS, Inc) are attached to the moveable plate to measure its displacement. The moveable plate is kept on the track with load bearing rollers in which the only degree of freedom is along the longitudinal axis (x-axis) of the bumper crusher. Hence, the displacement transducers provided data on the deformation of the bumper system along the x-axis. During the measurement of the QS F-D data, video and sound information were also recorded.

The test bumpers were mounted on the steel plates of the bumper crusher using their original equipment brackets and attachment hardware. Rigid attachments for the bumper brackets were bolted on the steel plates of the bumper crusher, and the bumpers and brackets were bolted to these attachments. These rigid attachments represented the frame horns or the unibody structure and were much stiffer than the bumpers and their mounting brackets. Therefore, during the QS F-D measurements the only structures that underwent measurable deformation were the bumpers.



**Figure 1. A photograph of the bumper crusher, the device used to quasi-statically crush the bumpers of a bumper system into each other.**

Bumpers for older vehicles were obtained from salvage yards, and the bumpers for newer vehicles were obtained from dealers. The bumpers from the salvage yards were inspected to make sure there was no damage. Only original equipment bumpers (OEM) were used. The QS F-D measurements were performed with the bumper covers and any energy absorbing components in place and measurements were conducted up to a maximum deformation that produced notable damage to at least one of the bumpers. The displacement transducers documented the overall deformation to the system and video documented the overall and localized deformations. The sound information was useful in that many of the bumper component failures created noise and this audio data could be correlated with the force data to determine the failure force of a particular component.

Bumper System A was composed of the rear bumper of a 1994 Toyota Tercel and the front bumper of a 2003 Chevrolet Express Van. The Tercel's rear bumper is shown in [Figure 2](#) with the bumper cover removed. The Tercel's rear bumper has a steel impact bar (bumper beam) with four steel cover supports welded to the rear upper surface which support the bumper cover along with two small expanded polypropylene (EPP) pads. The two inboard supports extend rearward approximately 3.8 cm (1.5 inches) from the surface of the

impact bar. The Tercel's rear bumper had a cover made of polypropylene (PP). The Chevy Express Van's front bumper has a steel face bar with a PP cover on the top 5 cm (2 in.) of the front surface of the face bar, and, when the two bumpers engaged, the cover supports on the Tercel's bumper made the first hard contact with the van's bumper. The bumpers of Bumper System A are shown on the bumper crusher in [Figure 3](#) prior to a QS F-D measurement.



**Figure 2. The top photograph shows the impact bar on the rear bumper of a 1994 Toyota Tercel. The lower photograph shows the left side cover supports welded to the top rear surface of the impact bar which support the bumper cover (not shown).**

Bumper System B was composed of the rear bumper of a 2002 Honda Civic Sedan and the front bumper of a 2007 Ford Escape. The impact bars for Bumper System B are shown on the bumper crusher prior to a QS F-D measurement in the upper photograph in [Figure 4](#). The Civic bumper had a convex steel impact bar with a rectangular shaped steel section welded to the center that extended approximately 2 cm (0.8 in) from the impact bar. As shown in the lower photograph in [Figure 4](#), an EPP impact absorber fitted over the rear surface of the impact bar with a cutout for the center extension. The impact absorber had a thickness that varied

from approximately 1.5 to 2.5 cm (0.6 to 1.0 in). The steel brackets that attached the impact bar to the unibody structure of the Civic were welded to the impact bar. The Civic's rear bumper had a PP bumper cover. The 2007 Ford Escape had a convex steel impact bar and the brackets that attached the impact bar to the unibody structure were welded around the impact bar. The Escape's front bumper had no impact absorber located between the impact bar and the PP cover.

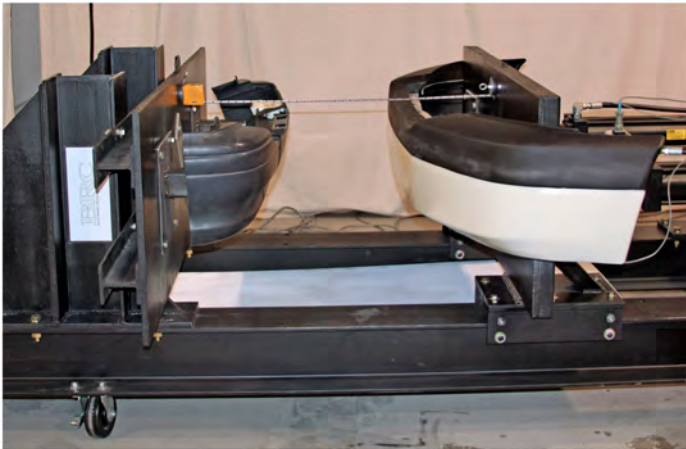


**Figure 3. Bumper System A prior to a QS F-D measurement with the Tercel's bumper on the fixed plate (left side) and the Chevy Express Van's bumper on the moveable plate (right side).**

Bumper System C was composed of the rear bumper of a 2008 Honda Civic Sedan and the front bumper of a 2005 Kia Sedona. The impact bars for Bumper System C are shown on the bumper crusher prior to a QS F-D measurement in the upper photograph in [Figure 5](#). The Civic's bumper had a convex aluminum impact bar with a rectangular extension welded to the center that extended approximately 1 cm (0.4 in) from the rear surface of the impact bar. As shown in the middle photograph of [Figure 4](#), there was an EPP impact absorber that covered part of the rear surface of the impact bar. The impact absorber had a thickness that ranged from approximately 1.0 to 1.5 cm (0.4 to 0.6 in). The mounting brackets were steel and were bolted onto the impact bar. The Civic's bumper had a PP cover. The Sedona's bumper had a glass mat thermoplastic (GMT) impact bar. As shown in the lower photograph of [Figure 5](#), a white EPP impact absorber covered the entire rear surface of the impact bar and extended over the top surface as well. The section of the impact absorber that covered the rear surface of the impact bar had a thickness that ranged from approximately 1.0 to 2.0 cm (0.4 to 0.8 in). A PP cover support on the impact bar's top surface extended above the impact absorber and provided support for the Sedona's PP bumper cover. The steel mounting brackets were attached to the GMT impact bar with bolts.

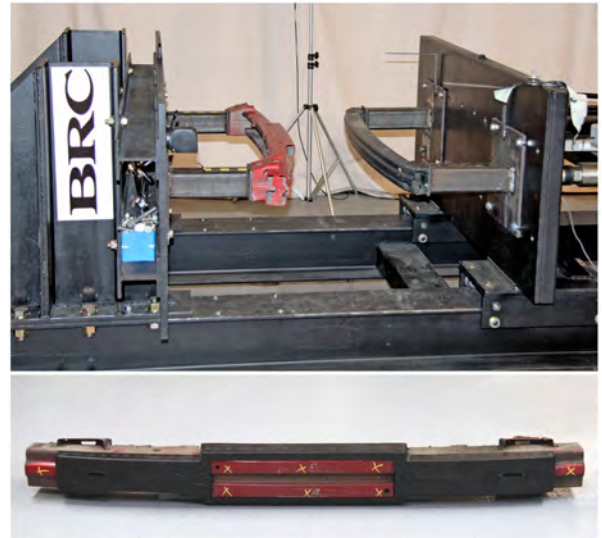


**Figure 4. The top photograph shows the impact bars of Bumper System B prior to a QS F-D measurement, with the Civic's impact bar on the fixed plate (left side) and the Escape's impact bar on the moveable plate (right side). The lower photograph shows the Civic's black impact absorber on the impact bar.**

## CRASH TESTS

A series of crash tests were performed with each bumper system. In each crash test the dynamic F-D characteristics of the bumper system and the vehicle dynamics were measured. The bullet vehicle in each crash test was a buck that had the front bumper of the bumper system attached to it. The target vehicle in each crash test was a production vehicle with an OEM rear bumper. The target vehicle was always stationary pre-crash with the transmission in neutral and the bullet vehicle, the buck, was accelerated to the impact speed by rolling down a ramp. A schematic of the test setup for the crash tests is shown in [Figure 6](#).

The buck was made from a pickup's chassis and suspension and the buck's weight could be adjusted to represent the weight of the vehicle whose bumper was mounted on the front. The adjustable weights were rigidly attached to the frame of the buck. The buck had a vertically oriented steel plate rigidly attached to the front of the frame and six load cells (Model 1210AO, Interface, Inc.) were attached to this plate. A second steel plate, the bumper plate, was attached to the other end of the load cells at the front of the buck. The front bumper of the bumper system was mounted on the bumper plate with attachment hardware similar to the hardware used on the bumper crusher. The front bumper on the buck was positioned on the bumper plate such that when it contacted the rear bumper on the target vehicle, it was in the same orientation as the bumpers in the QS F-D measurements. A string potentiometer (T2A, Celesco, Inc) was attached to the bumper plate and the string was attached to a moveable rod that extended past the bumper on the buck.

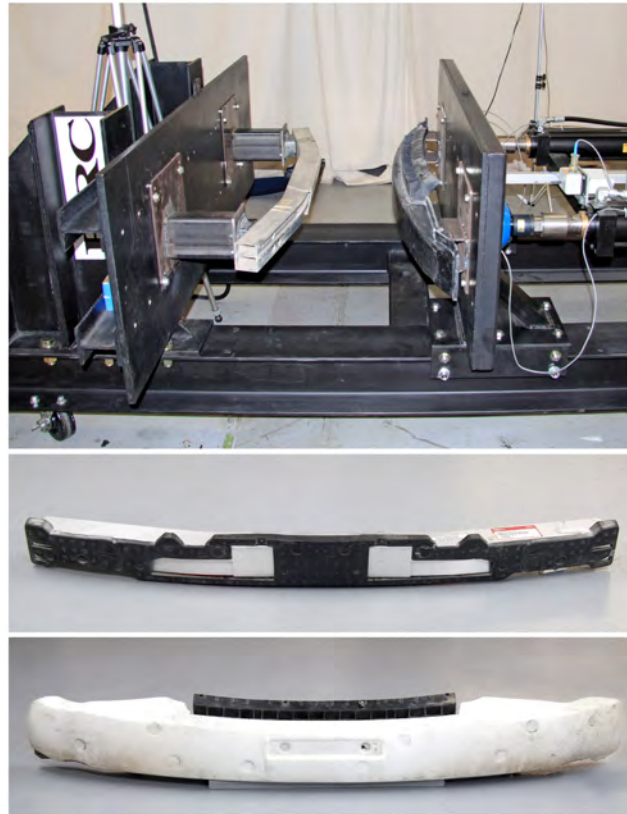


**Figure 5.** The top photograph shows the impact bars of Bumper System C prior to a QS F-D measurement, with the Civic's aluminum impact bar on the fixed plate (left side) and the Sedona's impact bar on the moveable plate (right side). The middle photograph shows the Civic's black impact absorber on the impact bar. The lower photograph shows the Sedona's white impact absorber on the impact bar.

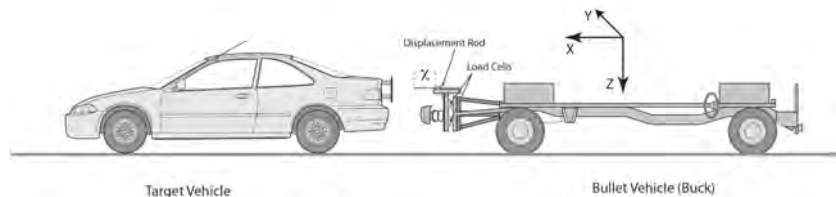


**Figure 6.** A schematic of the test set up used in the low-speed crash tests.

During a crash the rod contacted a flat plate above the rear bumper of the target vehicle, as shown in Figure 6, before the bumpers contacted each other and the relative movement of the rod with respect to the bumper plate during the crash was measured by the string pot. During the crash the displacement sensor measured the distance ( $\chi$ ) between the plate on the rear of the target vehicle and the bumper plate on the buck, as shown in Figure 6. Since the rod contacted the plate on the target vehicle before the bumpers made contact,  $\chi$  is set to zero at the time an impact force is recorded by the load cells and  $\chi$  represents the longitudinal deformation of the bumper system.

The buck had tri-axial accelerometers rigidly attached to the frame and the target vehicle had tri-axial accelerometers

rigidly attached to the floor pan and the unibody structure under the vehicle. Redundant accelerometers were used in case one set of accelerometers failed during a crash test. The x-axis is along the direction of travel of the bullet vehicle. During a crash test all sensor signals were sampled at a frequency of 5000 Hz (16-channel TDAS-PRO, DTS, Inc. and 16-channel 6210 NI, Inc.) and filtered at 100 HZ (SAE J211 CFC60). The impact speed of the bullet vehicle was measured with an infra-red sensor (SM312LVMHS, Banner, Inc.) and retro-reflective tape (Banner, Inc.) and also with high-speed digital video recordings (1000 frames/sec). High speed and normal video cameras were used to document the deformation of the bumpers and the vehicle behavior during the crash tests.

The impact forces during a crash test were calculated from three different transducer data sets and compared to ensure that the transducers operated properly during that crash test. The three transducer data sets were the load cells on the bullet vehicle and the x-axis accelerometers on the bullet and target vehicles. The load cells have a mass between their location on the buck and the surface where the impact force is acting on each bumper. The mass ( $M_{BP}$ ) is made up of the bumper plate (139.5 kg, (307.5 lbs)), the bumper hardware and the steel that represents the frame or unibody structure of the bullet vehicle that is bolted onto the bumper plate. The force required to accelerate  $M_{BP}$  must be added to the crash forces measured by the load cells ( $F_{LC}(t)$ ) in order to obtain the impact force ( $IF_{LC}(t)$ ) acting on the bumpers;

$$IF_{LC}(t) = |A_B(t)| M_{BP} + F_{LC}(t) \quad (1)$$

where  $t$  is time and  $A_B(t)$  is the x-axis acceleration of the buck (bullet vehicle). The absolute value of  $A_B(t)$  is used for this analysis because the accelerations of the buck were negative in the crash tests, but all forces have been made positive for the comparison.  $F_{LC}(t)$  is the sum of the six load cells on the buck. The mass of the target and bullet vehicles and the mass of the plate, bumper and hardware on the front of the buck used with each bumper system are listed in [Table 2](#).

**Table 2. The masses of the target vehicles, bullet vehicles and attachment hardware.**

Bumper System	Target Vehicle Mass ( $M_T$ )	Bullet Vehicle Mass ( $M_B$ )	$M_{BP}$
A	977 kg	2453 kg	190 kg
B	1257 kg	1490 kg	167 kg
C	1330 kg	1874 kg	161 kg

The impact forces calculated using the accelerometer data from the target vehicle ( $IF_T(t)$ ) and the bullet vehicle ( $IF_B(t)$ ) are;

$$IF_T(t) = M_T A_T(t) \quad (2)$$

$$IF_B(t) = M_B |A_B(t)| \quad (3)$$

where  $M_T$  is the mass of the target vehicle,  $M_B$  is the mass of the bullet vehicle and  $A_T(t)$  is the x-axis acceleration of the target vehicle. [Equations \(Eqs.\) 2 and 3](#) assume that the target and bullet vehicles are rigid-bodies and therefore, the measured accelerations represent the uniform acceleration of the entire mass of the vehicle.

The velocities of the bullet vehicle ( $V_B(t)$ ) and the target vehicle ( $V_T(t)$ ) during a crash were obtained by integrating the x-axis accelerations of the bullet and target vehicle and using the initial velocities;

$$V_B(t) = V_{\text{impact}} + \int A_B(t) dt \quad (4)$$

$$V_T(t) = \int A_T(t) dt \quad (5)$$

where  $V_{\text{impact}}$  is the impact velocity of the bullet vehicle and the integration is from the start of the crash to time  $t$  in the crash. As previously mentioned, the target vehicle was always stationary prior to impact by the bullet vehicle. [Eqs. 4 and 5](#) assume that the target and bullet vehicle are rigid masses and the measured acceleration represents the uniform acceleration of the entire mass of the vehicle.

An analysis of the energy available for crush in a collision was used to evaluate the performance of the displacement sensor and the load cells on the buck in each crash test. In order to do this evaluation, the energy available for crush was determined using two different methods. The first method was to use the pre-crash and post-crash velocities of the vehicles to determine the energy available for crush ([10](#)). The energy available for crush ( $E_{\text{afc}}$ ) using the pre-crash and post-crash velocities is;

$$E_{\text{afc}} = 1/2 M_B M_T V_{\text{impact}}^2 / (M_B + M_T) \quad (6)$$

The second method was to determine the energy required to crush the bumpers to the maximum deformation in the crash tests, which should be equal to  $E_{\text{afc}}$  ([1](#)). The work done deforming the bumpers up to the maximum crush is called the energy available for crush measured in the crash test ( $E_{\text{afcm}}$ ) and was calculated for each crash test, thus;

$$E_{\text{afcm}} = \int IF_{LC}(\chi) d\chi \quad (7)$$

where  $\chi$  is the deformation of the bumper system (see [Figure 6](#)) and the integration was performed from initial contact up to the maximum deformation. The magnitude of  $E_{\text{afcm}}$  should be close to  $E_{\text{afc}}$  if the displacement sensor and the load cells operated properly in each crash test.

The impact speeds of the bullet vehicle in each series of crash tests are shown in [Table 3](#). Each crash test is referred to by the bumper system letter and the crash test number for that bumper system. The impact speed in the crash tests for each bumper system was varied in order to look at the dynamic performance of the bumper system over a range of impact speeds. After the first crash test in a series the bumpers were checked for any deformation and replaced if damaged or

deformed. All impact bars, foam absorbers and brackets were replaced after the second crash test in a series.

**Table 3. Impact speed of the bullet vehicle in the crash tests for each bumper system.**

**Bumper System A**

Crash Test	Impact Speed
A1	1.0 m/s
A2	1.7 m/s
A3	2.5 m/s

**Bumper System B**

Crash Test	Impact Speed
B1	1.2 m/s
B2	3.0 m/s
B3	4.2 m/s

**Bumper System C**

Crash Test	Impact Speed
C1	0.9 m/s
C2	1.9 m/s
C3	2.3 m/s

**SIMULATION OF CRASH TESTS USING THE QUASI-STATIC FORCE-DEFORMATION DATA**

The crash tests were simulated by using the QS F-D compression data in the low-speed simulation model (1). The QS F-D compression data were used to represent the impact force-deformation (IF-D) characteristics of the bumper system during the compression phase of the simulated crash. The other inputs required for each simulation were the masses of the target and bullet vehicles, the impact speed of the bullet vehicle ( $V_{impact}$ ) and the coefficient of restitution ( $\epsilon_{test}$ ) measured in the crash test. In the simulation of a crash test, the compression phase of the crash ends when the bullet and target vehicles reach a common velocity and, to continue

the simulation, the model must calculate a rebound IF-D curve. The energy definition of the coefficient of restitution was used to calculate the rebound IF-D curve in the simulation of each crash test (1). The technique is shown graphically in Figure 7, which shows the IF-D curve used in the simulation of Crash Test A2. The compression phase of the IF-D curve ends at the point ( $D_{max}$ ,  $IF_{maxd}$ ), where  $D_{max}$  is the maximum deformation and  $IF_{maxd}$  is the impact force at maximum deformation. The  $\epsilon_{test}$  for each crash test was determined using the pre-crash and post-crash vehicle velocities measured in the crash test;

$$\epsilon_{test} = (V_T^* - V_B^*) / V_{impact} \tag{8}$$

where  $V_T^*$  and  $V_B^*$  are the post-crash velocities of the target and bullet vehicles. The energy returned to the vehicles during the rebound phase of the simulated crash ( $E_{afc}^*$ ) was determined using the energy definition of the coefficient of restitution;

$$E_{afc}^* = \epsilon_{test}^2 E_{afc} \tag{9}$$

where  $E_{afc}$  is the energy used to crush the bumpers up to  $D_{max}$  (1). In the simulations the work done to crush the bumpers up to the point ( $D_{max}$ ,  $IF_{maxd}$ ) equals  $E_{afc}$  (Eq. 6) because the simulation model follows Newton's Laws throughout the simulated crash and no energy is lost in the rigid vehicles. The meanings of  $E_{afc}^*$  and  $E_{afc}$  are shown graphically in Figure 7. The rebound IF-D curve is taken to be a straight line that starts at ( $D_{max}$ ,  $IF_{maxd}$ ) and has a slope that allows Eq. 9 to be satisfied. The slope of this line is;

$$\text{Slope} = IF_{maxd}^2 / (2 \times E_{afc}^*) \tag{10}$$

Figure 7 shows the rebound IF-D curve calculated for the simulation of Crash Test A2 using this method.

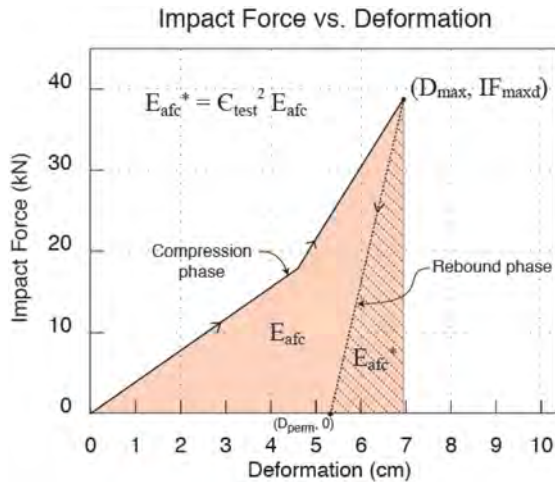


Figure 7. Illustration that shows the compression and rebound IF-D curves used in the simulation of Crash Test A2.  $E_{afc}$  is the shaded area and  $E_{afc}^*$  is the hatched area.

## RESULTS

### QUASI-STATIC FORCE-DEFORMATION MEASUREMENTS

Each QS F-D curve is composed of a compression phase and a rebound phase. The force is the sum of both load cells of the bumper crusher. The compression phase starts at zero deformation and continues until the bumper system is compressed to its maximum deformation. The rate of compression was approximately 1.3 cm/s (0.5 in./s). The rebound phase occurs when the pressure in the hydraulic cylinders is reduced and the elastic rebound forces in the bumpers push the bumpers apart. During the rebound phase the moveable plate had a speed of approximately 1.3 cm/s (0.5 in./s). When the force reaches zero the bumper system is at its permanent deformation. The point of maximum deformation in each curve represents the end of the compression phase of the curve and the beginning of the rebound phase of the curve.

The QS F-D measurements of Bumper System A are shown in Figure 8. The first measurement is called QS A1 and the second is QS A2, a naming convention that will be used for all the quasi-static measurements.

The curves for QS A1 and QS A2 are almost identical. The compression phases of QS F-D curves for Bumper System A were approximated with the straight lines shown in Figure 8 for the simulations of Crash Tests A1, A2 and A3.

The condition of the bumpers after the QS A1 measurement is shown in Figure 9. There was very little deformation to the rear bumper of the Toyota Tercel and most of the deformation that was measured in the system was due to the deformation of the Chevy Express Van's front bumper. The two small concavities or depressions in the middle of the

van's face plate were caused by the bumper cover supports on the top of the Tercel's impact bar. The upper surface of the van's face bar was pushed rearward relative to its mounting points and, as viewed from the left side of the van, the face bar rotated in a clockwise direction, as shown in Figure 9.

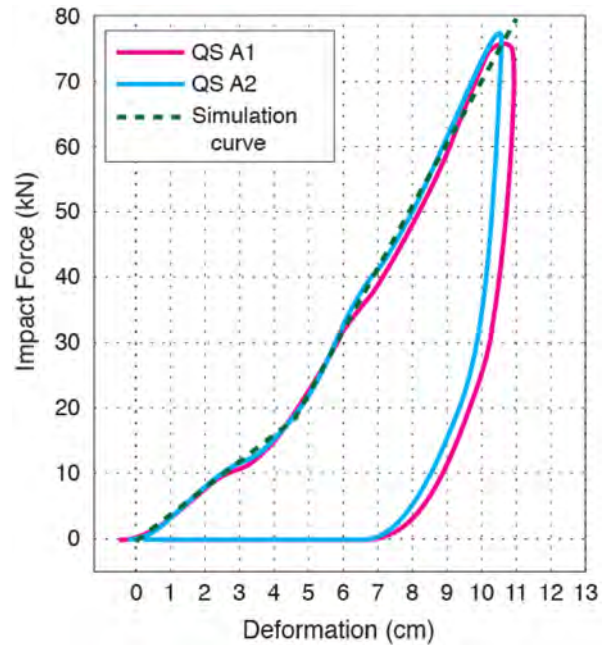
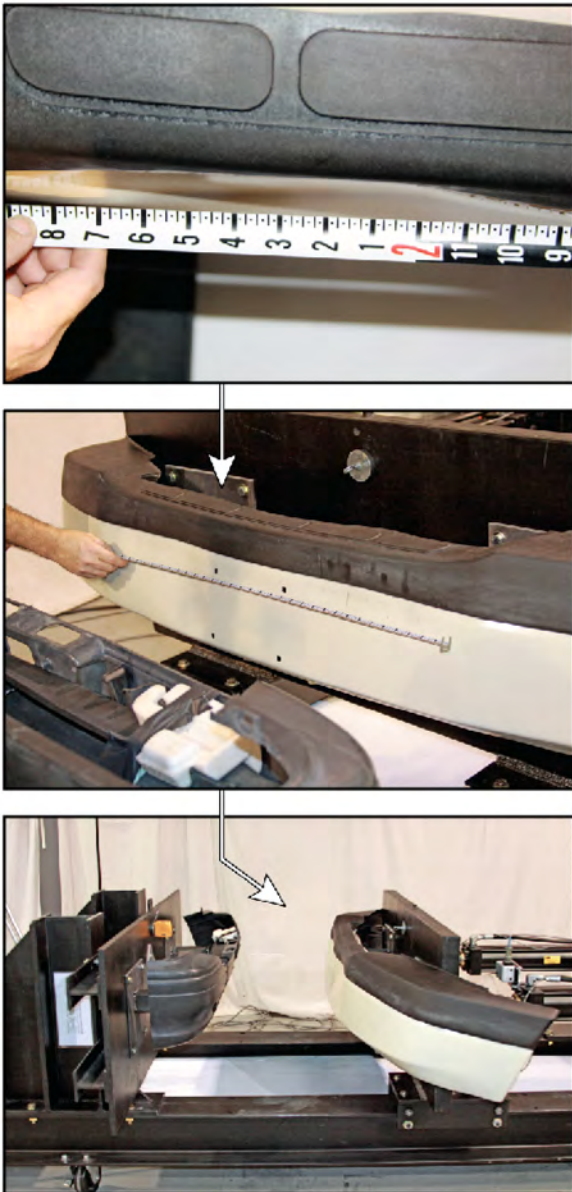


Figure 8. The QS F-D measurements made for Bumper System A. The compression IF-D curve used in the simulation is shown as dashed lines.

The compression phases of QS A1 and QS A2 each have two small concavities. The first concavity starts at a force of approximately 10 kN (2,248 lbs) and was caused by the penetration of the brackets on the top of the Tercel's rear bumper into the face bar of the Chevy Express Van. The second concavity starts at a force of approximately 35 kN (7,868 lbs) and occurred when the top of the van's face bar was pushed rearward and the face bar began to rotate about its mounting brackets. When the measurement was stopped at approximately 76 kN (17,085 lbs), the maximum deformation was approximately 10.5 cm (4.1 in.). At the end of the rebound phase of the measurement, the permanent deformation was approximately 7 cm (2.8 in.). The compression phases of the QS F-D curves for Bumper System A were approximated with the two straight lines shown in Figure 8 for use in the simulations of Crash Tests A1, A2 and A3.



**Figure 9. Bumper System A after the QS A1 measurement. The Express Van's front bumper, on the right, has rotated in a clockwise direction as viewed from the left side of the vehicle.**

The QS F-D curves for Bumper System B, QS B1 and QS B2, are shown in Figure 10. QS B1 is composed of two different measurements that are named QS B1<sub>1</sub> and QS B1<sub>2</sub>. The first measurement, QS B1<sub>1</sub>, was stopped after the bumper system had deformed approximately 17 cm (6.7 in.) during the compression phase of the measurement. During the rebound phase the system rebounded 4 cm (1.6 in.) and the permanent deformation was approximately 13 cm (5.1 in.). These bumpers were compressed again shortly after this measurement was completed in order to look at the continuity of the F-D measurement. The compression phase of this curve, QS B1<sub>2</sub>, followed the rebound curve of QS B1<sub>1</sub> up

until a force of approximately 90 kN (20,232 lbs) and then the forces remained fairly constant at 95 kN (21,356 lbs) as the bumpers were compressed further. In QS B1<sub>2</sub> the compression phase was stopped at a maximum deformation of 22 cm (8.7 in.). During the rebound phase of QS B1<sub>2</sub> the bumpers rebounded 5 cm (2.0 in.) and the permanent deformation was approximately 17 cm (6.7 in.). New bumpers for Bumper System B were placed on the bumper crusher and a continuous measurement was made up to a maximum crush of 23 cm (9.1 in.), QS B2. During the rebound phase of QS B2 the bumpers rebounded approximately 5 cm (2.0 in.) and the permanent deformation was approximately 18 cm (7.1 in.). The combination of the QS B1<sub>1</sub> and QS B1<sub>2</sub> curves was similar in shape to the QS B2 curve.

The shape of the compression phase of the QS F-D curves for Bumper System B reflects three different events which are delineated by reductions in force in the compression phase of the curve. These force reductions occur at the same amount of deformation in the first and second measurement, but the drop-offs in force occurred at higher forces in the second test than the first test. The first drop-off occurred just after approximately 7.5 cm (3.0 in.) of deformation when the impact bar of the Ford Escape began to yield. In the first measurement the impact bar began to yield at a force of approximately 36 kN (8,093 lbs) and in the second measurement it occurred at a force of approximately 49 kN (11,015 lbs), a difference of 13 kN (2992 lbs). Once the impact bar for the Escape yielded, the loading between the two bumpers was at the brackets. The second event occurred at a deformation of approximately 12 cm (4.7 in.), when the Escape's brackets began to yield. In the first measurement the brackets began to yield at a force of approximately 66 kN (14,837 lbs) and in the second measurement it occurred at a force of approximately 79 kN (17,759 lbs), a difference of 14 kN. The force difference between the two measurements remained fairly constant between the first and second yielding event. The third event was the yielding of the brackets that mounted the Civic's impact bar to the unbody structure. This occurred at approximately 16 cm (6.3 in.) of deformation in the first test and 18 cm (7.1 in.) of deformation in the second test. Once the Civic's brackets began to yield the force remained fairly constant in both tests at approximately 90 kN (20,232 lbs). The damage to the bumpers after the QS B2 measurement is shown in Figure 11.

The difference between the two QS F-D measurements for Bumper System B involved the performance of the Escape's bumper, not the Honda's bumper. In QS B1<sub>1</sub> the Escape's impact bar and mounting brackets, which surround the impact bar, began to plastically deform at a lower force than in QS B2. It is not clear why the difference occurred, but it may reflect variability in the composition of the steel used to make the Escape's impact bar. The mounting brackets for the Civic's bumper began to plastically deform at approximately the same force in QS B1<sub>1</sub> and QS B2. The QS

F-D measurement with the highest forces was used to simulate the crash tests and for Bumper System B this was QS B2. This approach is used to ensure that the  $\Delta V$  and acceleration estimates for a given amount of deformation in a simulation provide a conservative recreation of the crash, i.e. the greatest value of the  $\Delta V$  and the accelerations based on the available damage data. The compression phase of the QS B2 curve was approximated with the straight lines that are shown in Figure 10 for use in the simulations of Crash Tests B1, B2 and B3.

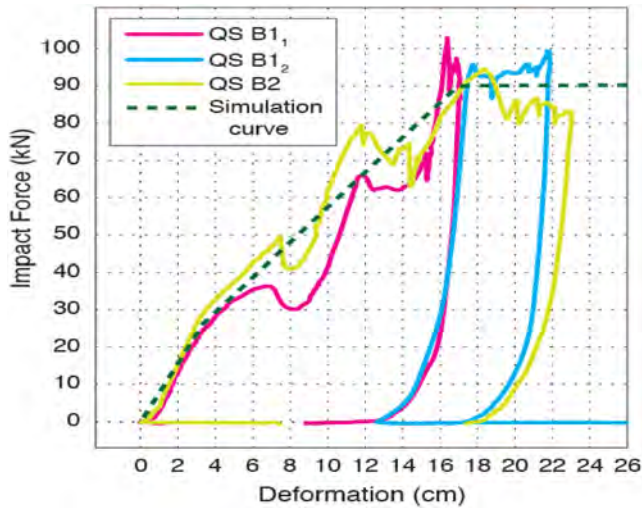


**Figure 10.** The QS F-D measurements made with Bumper System B. The first set of bumpers were compressed once and allowed to rebound (QS B1<sub>1</sub>) and then compressed again and allowed to rebound (QS B1<sub>2</sub>). The compression IF-D curve used in the simulation is shown as dashed lines.

The QS F-D curves measured for Bumper System C are shown in Figure 12. Initially, the compression curves for QS C1 and QS C2 were fairly linear with a slight increase in stiffness as the deformation increased. In both curves there was sharp drop in the compression force when the Sedona's impact bar fractured. In QS C1 the fracture occurred at a force of approximately 33 kN (7,418 lbs) and in QS C2 at approximately 38 kN (8,542 lbs). This difference in fracture force may have been due to differences in the composition of the GMT material that formed the Sedona's impact bars. As the bumpers were compressed further the force remained low, below 20 kN (4,496 lbs), until approximately 11 cm (4.3 in.) of deformation when the mounting brackets for the Sedona's and the Civic's bumpers began to load each other directly and the force increased with further deformation. In both tests the maximum deformation was approximately 15 cm (5.9 in.). The compression phase of QS C2, the measurement with the highest forces, was approximated with the straight lines shown in Figure 12 for the simulations of Crash Tests C1, C2 and C3.

The state of the impact bars for each bumper (bumper covers are not in place) after QS C1 is shown in Figure 13.

Most of the deformation occurred to the Sedona's bumper where there was a fracture at the center of the impact bar and fractures around the mounting brackets. There was no significant deformation of the Civic's impact bar and mounting brackets after the QS C1 or QS C2 measurements.

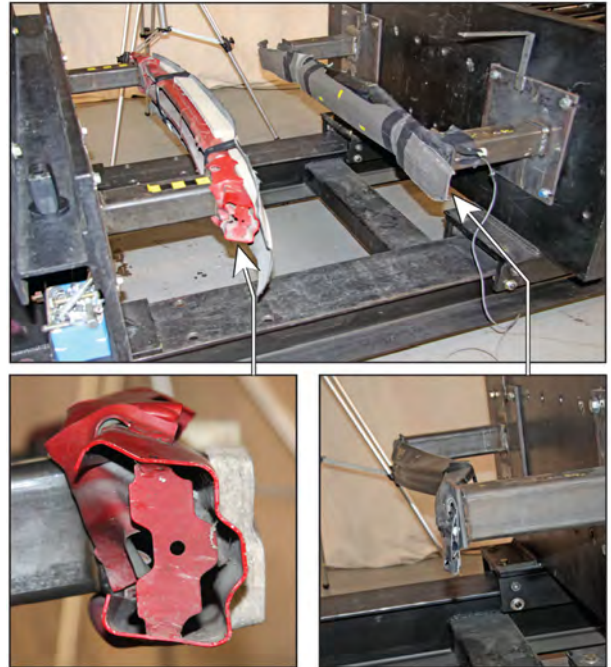


**Figure 11.** Photographs that show the damage to Bumper System B during the measurement of QS B2. The Civic's impact bar is red and the Escape's impact bar is black.

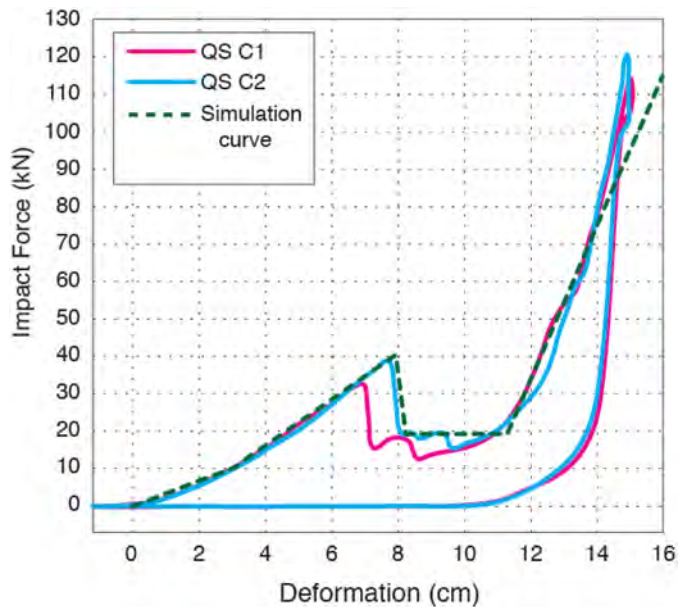


**Figure 12.** The QS F-D measurements for Bumper System C.



**Figure 13.** The impact bars for the bumpers in System C after QS C1. The Sedona's impact bar fractured at the center and around the mounting brackets.

## CRASH TESTS RESULTS

The vehicle velocities calculated from the vehicle accelerations (Eqs. 4 and 5),  $IF_{LC}(t)$  (Eq. 1) and the deformation of the bumper system ( $\chi$ ) for each crash test are shown in Figures 14, 15 and 16 as a function of time. All of the velocity curves are relatively smooth except for the velocities in Crash Test C3, where the impact bar for the Sedona's front bumper fractured and the impact forces were significantly reduced for a short time. The decrease in velocity experienced by the target vehicle and the small increase in velocity experienced by the buck are thought to reflect the non-rigid body behavior of the Civic and the buck.

One of the checks on the sensor data for each crash test was to confirm that the maximum deformation occurred when the bullet and target vehicles reached a common velocity. The time the vehicles achieved a common velocity is the intersection of the bullet and target vehicle velocities in Figures 14, 15, 16. In all of the crash tests shown in Figures 14, 15, 16, the maximum deformation occurs very close in time to the common velocity. This check is one indicator that the accelerometers, the displacement sensor and the load cells all functioned properly during each test.

A second check of the transducer's performance and the rigid-body assumption was to compare the impact forces calculated from the load cell and the accelerometer data (Eqs. 1, 2 and 3). These impact forces are shown in Figures 17, 18 and 19 for all of the crash tests. The impact forces calculated with the buck's accelerations,  $IF_B(t)$ , are presented as an absolute value in order to make the comparison with  $IF_T(t)$  and  $IF_{LC}(t)$ . The impact forces calculated with the load cell data and the accelerometer data are similar in each crash test, except for Crash Test C3. In the force calculations for the other crash tests, there were slight differences in accelerometer-based forces and the load-cell based forces. The acceleration-based impact forces, especially  $IF_T(t)$ , were consistently higher than  $IF_{LC}$  during the first part of the compression phase of the crash and lower than  $IF_{LC}$  during the rebound phase. Vibrations in the target vehicle, which is a

production vehicle, became more pronounced as the impact speed increased in each test series and this is reflected in the  $IF_T(t)$  data for all of the bumper systems. In Crash Test C3  $IF_T(t)$  and  $IF_B(t)$  varied significantly from  $IF_{LC}(t)$ . All of these differences are thought to reflect the target vehicle, and to a lesser extent the buck, not behaving as a rigid-bodies. This idea is presented in more detail in the discussion section.

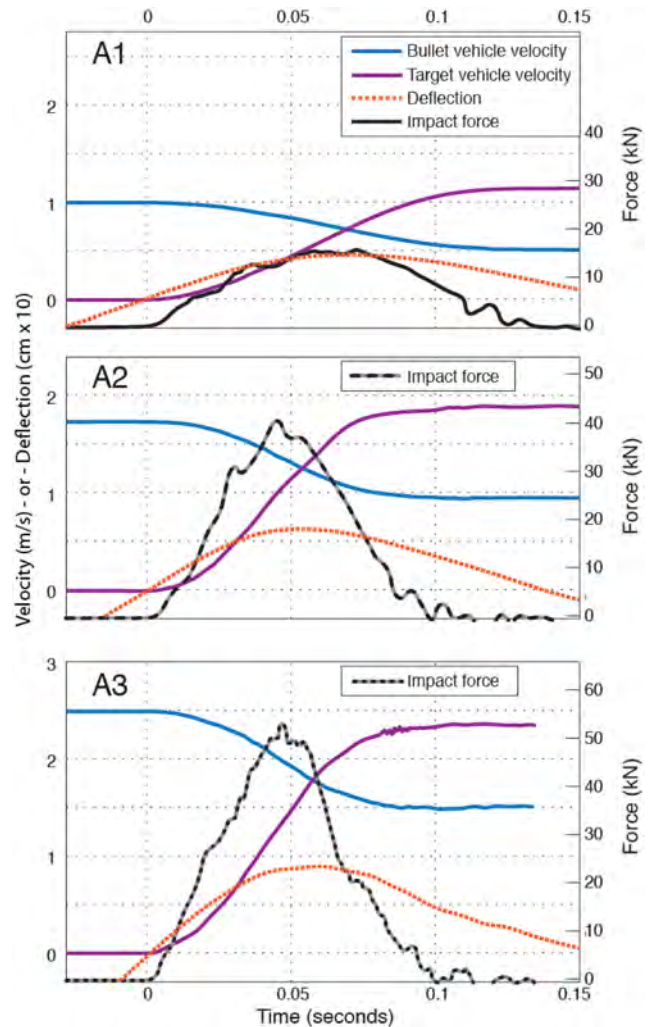


**Figure 14.** Vehicle velocities, impact forces and deformations measured in Crash Tests A1, A2 and A3.

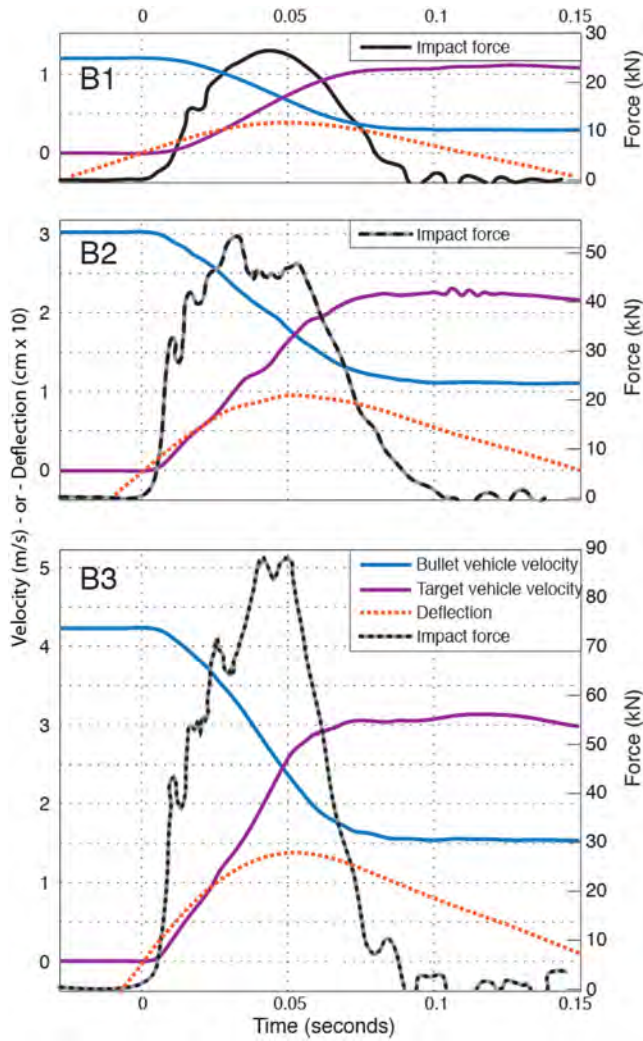


Figure 15. Vehicle velocities, impact forces and deformations measured in Crash Tests B1, B2 and B3.

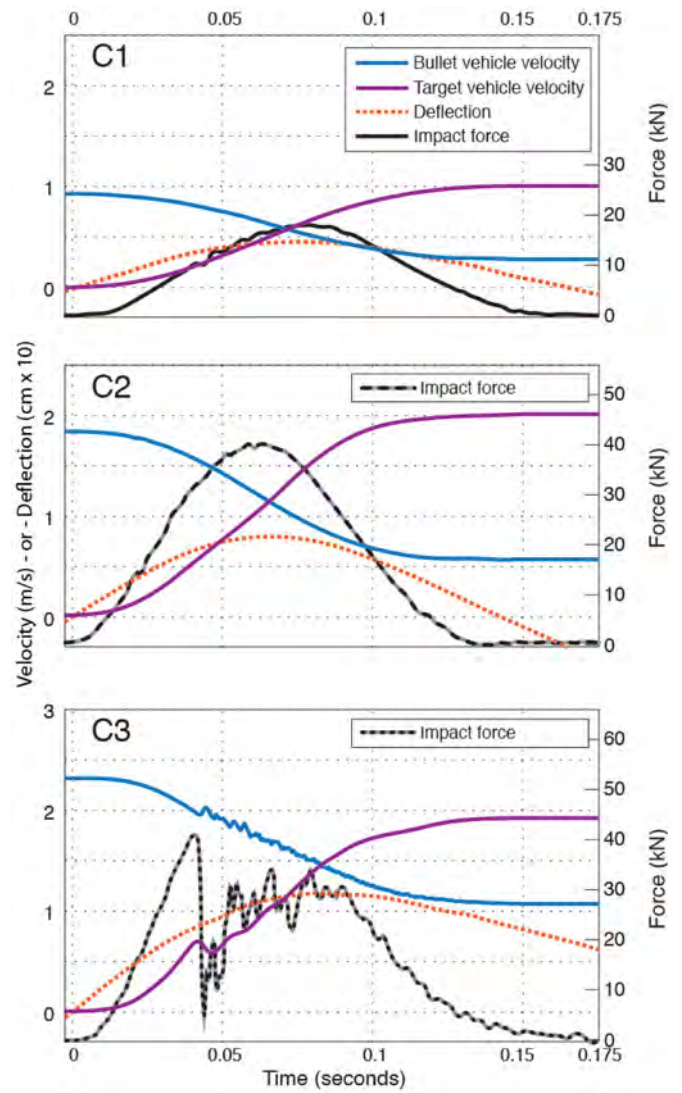


Figure 16. Vehicle velocities, impact forces and deformations measured in Crash Tests C1, C2 and C3.

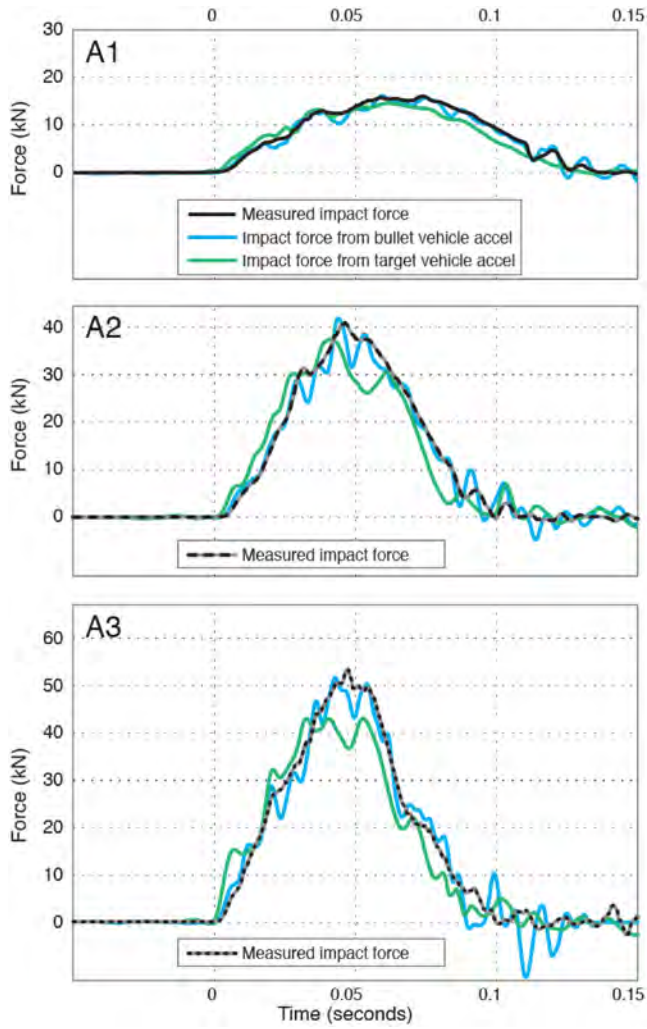


Figure 17. The measured impact force and the impact forces calculated using the vehicle accelerations in Crash Tests A1, A2 and A3.

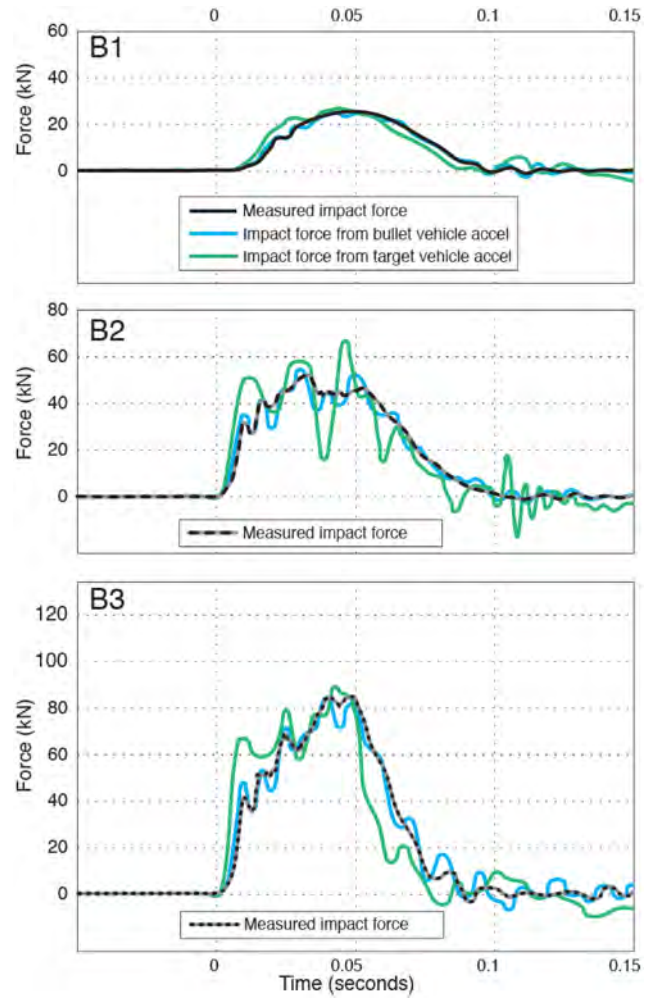


Figure 18. The measured impact force and the impact forces calculated using the vehicle accelerations in Crash Tests B1, B2 and B3.

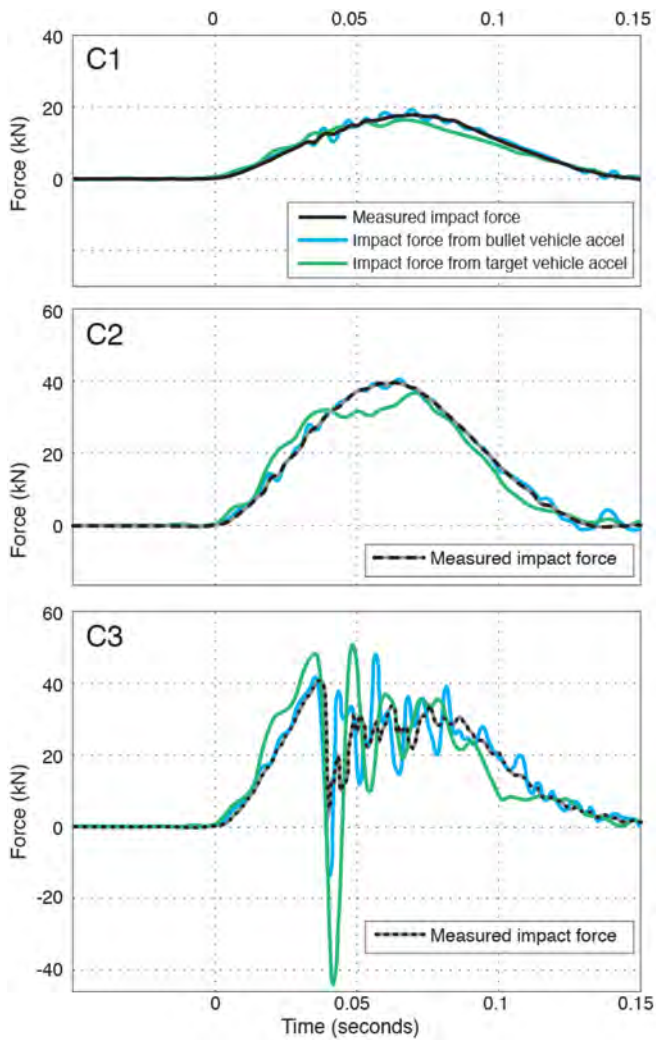


Figure 19. The measured impact force and the impact forces calculated using the vehicle accelerations in Crash Tests C1, C2 and C3.

The third method to check the accuracy of our crash tests and a method directly related to the measurement of the IF-D data was the comparison of the energy available for crush calculated with the pre and post-crash velocities ( $E_{afc}$ ) and the dynamic F-D data collected during the crash ( $E_{afcm}$ ). The values of  $E_{afc}$  and  $E_{afcm}$  for each crash test are given in Table 4 along with the percent difference ( $(E_{afcm} - E_{afc}) / E_{afc} * 100\%$ ). The similarity between  $E_{afc}$  and  $E_{afcm}$  indicates that the displacement sensor and the load cells performed well during the crash test. The good comparison between the  $E_{afc}$  and  $E_{afcm}$  in Table 4 also indicates that our assumption that the vehicles behave as rigid bodies is valid, at least in terms of the crush energy, for these impact speeds.

Table 4. Comparison of the energy available for crush calculated using the pre-crash and post-crash vehicle velocities ( $E_{afc}$ ) and the measured crush energy at maximum deformation ( $E_{afcm}$ ) in each crash test and the percent difference.

**Bumper System A**

Crash Test	$E_{afc}$ (N•m)	$E_{afcm}$ (N•m)	% Dif.
A1	351	351	0.0
A2	1060	1020	-3.8
A3	2172	2010	-7.5

**Bumper System B**

Crash Test	$E_{afc}$ (N•m)	$E_{afcm}$ (N•m)	% Dif.
B1	483	456	-5.6
B2	3122	3159	1.2
B3	6125	6219	-0.1

**Bumper System C**

Crash Test	$E_{afc}$ (N•m)	$E_{afcm}$ (N•m)	% Dif.
C1	356	347	-2.5
C2	1407	1318	-6.3
C3	2216	2200	-0.7

The dynamic and QS F-D curves for the bumper systems are shown in Figures 20, 21 and 22. The dynamic curves are IF<sub>LC</sub> graphed as a function of  $\chi$  for each crash test. For each bumper system, the peak force and the maximum deformation increase as the impact speed increases. In general there is very good agreement between the compression phase of the QS F-D curves and compression phase of the dynamic curves. The dynamic curves are influenced by the vibrations in the vehicles. The dynamic curves for Crash Test A1 and A2 appear to have the first concavity seen in the quasi-static curves. The curve for Crash Test A3, which has a peak force of approximately 53 kN (11,914 lbs), appears to have both concavities, although the second inflection point is at approximately 26 kN (5,845 lbs),

which is below the force, 35 kN (7,868 lbs), in QS A1 and QS A2. The rebound curve for all the crash tests for Bumper System A appear to have a slope similar to the slope of the rebound phase of the quasi-static tests at the same force level.

The dynamic and QS-FD curves for Bumper System B are shown in Figure 21, but only the QS B2 curve is shown in order to keep the graph more readable. The compression phase of the dynamic F-D curves for Bumper System B was generally similar to the QS F-D curves. In Crash Test B1 there was no damage to either impact bar. In Crash Test B2 the inflection point in the dynamic curve at approximately 52 kN (11,690 lbs) appears to be the force where the impact bar for the Ford Escape's front bumper began to yield. In Crash Test B3 the inflection point at 43 kN (9,666 lbs) appears to be where the Escape's impact bar began to yield and the inflection point at approximately 70 kN (15,736 lbs) appears to be where the Escape's mounting brackets begin to yield. In Crash Test B3, the vehicles reached a common velocity before there was significant deformation of the Civic's mounting brackets. The rebound curve for B1 has a slope similar to the QS compression curve at the same force and the rebound curves for B2 and B3 have a slope similar to the QS rebound curve at the same force.

As shown in Figure 22, the compression phase of the dynamic F-D curves in Crash Tests C1 and C2 were virtually identical to the quasi-static curves. The peak force in Crash Test C2 (impact speed = 1.9 m/s (6.1 ft/s)) was approximately 38 kN (8542 lbs) but the impact bar on the Sedona's front bumper did not fracture. In Crash Test C3 (impact speed = 2.3 m/s (7.6 ft/s)), the peak force was slightly greater than 40 kN (8992 lbs) when the impact bar fractured. Even after the impact bar fractured the dynamic loads were similar to the quasi-static forces at the same deformation, although there was significant variability in the QS and dynamic forces because the vibrations produced when the impact bar fractured influenced the dynamic forces. In Crash Tests C1 and C2 the rebound curves were parallel to the compression curves. In Crash Test C3 the slope of the rebound curve was similar to the slope of the quasi-static rebound curves at the same force.

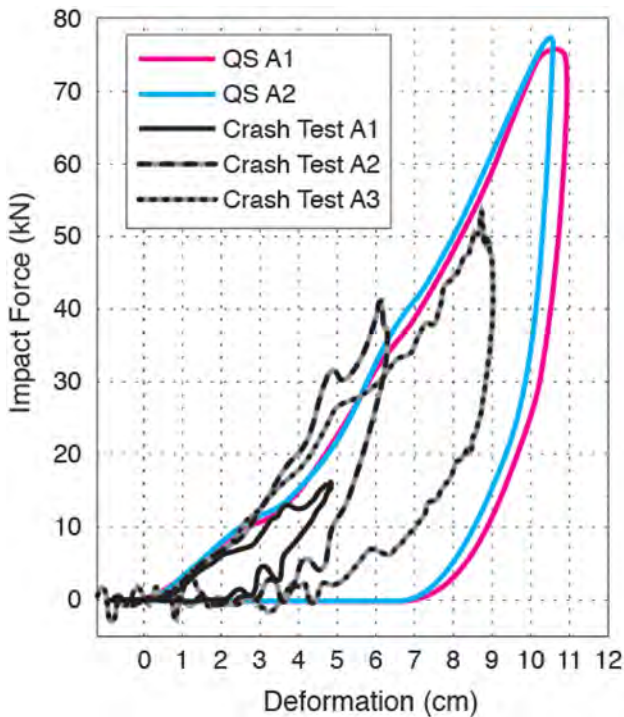


Figure 20. The QS and the dynamic F-D curves for Bumper System A.

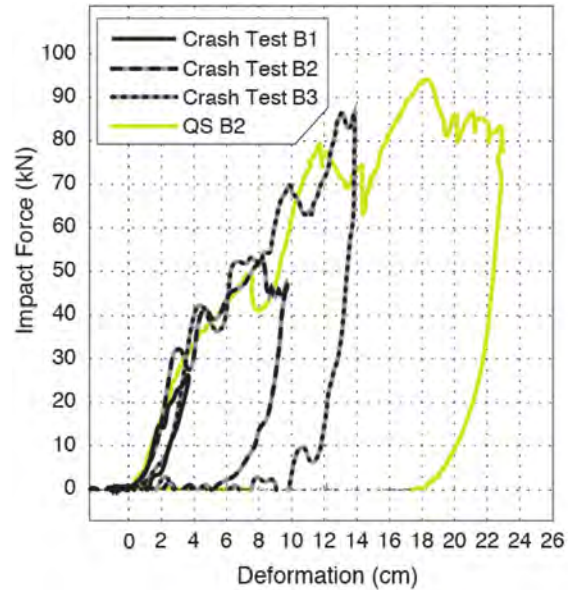


Figure 21. The QS and the dynamic F-D curves for Bumper System B.

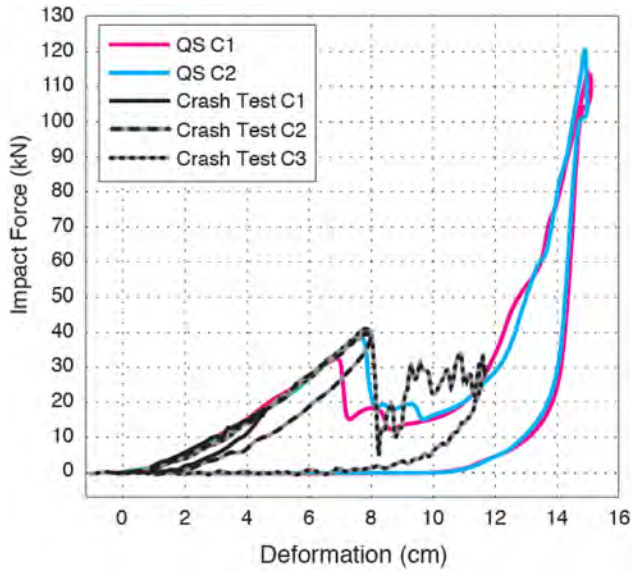


Figure 22. The QS and the dynamic F-D curves for Bumper System C.

## SIMULATIONS OF THE CRASH TESTS

Figures 23, 24 and 25 show the velocities calculated in the simulation of each crash test, along with the velocities calculated from the accelerometer data collected in the crash tests (Eqs. 4 and 5). The compression IF-D curve used to simulate the crash tests are shown in Figures 8, 10 and 12 for Bumper Systems A, B and C, respectively. The rebound IF-D curve for each simulation was calculated using Eqs. 8, 9 and 10. The velocity changes ( $\Delta V$ ) of the target and the bullet vehicles in the simulations are almost identical to the velocity changes of the vehicles measured in the crash tests. The calculated and measured crash pulse durations are very similar. The slight differences in the velocities prior to the vehicles reaching a common velocity reflect the compression phase of the IF-D curve used in the simulation, but the simple linear fit of the QS F-D curves (Figures 8,10 and 12) provides a good approximation of the impact forces produced in the actual crash.

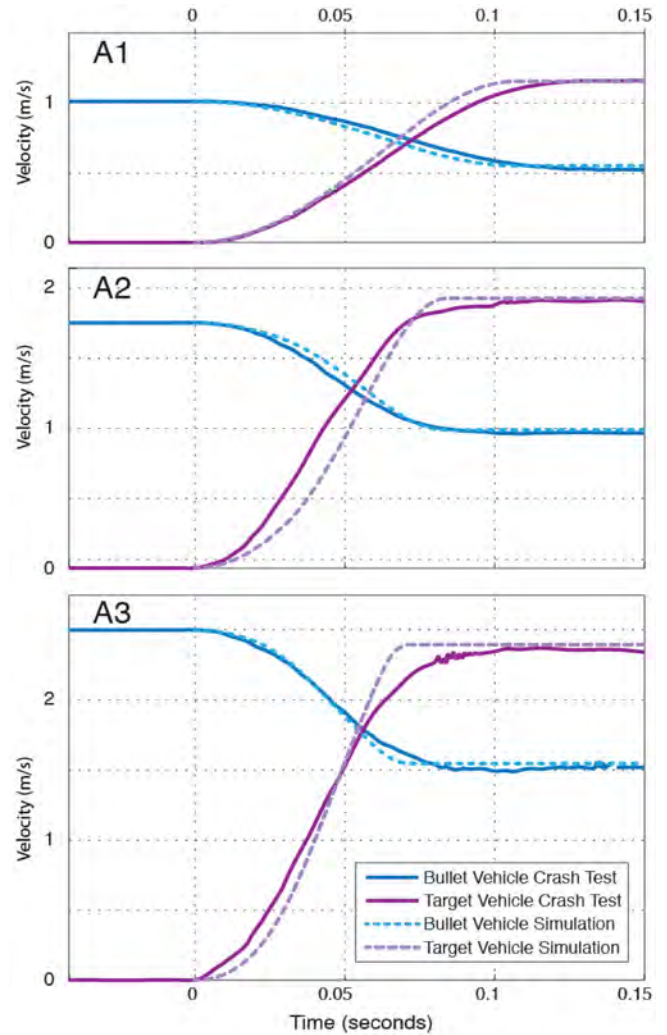


Figure 23. The velocities calculated in the simulations of Crash Tests A1, A2 and A3.

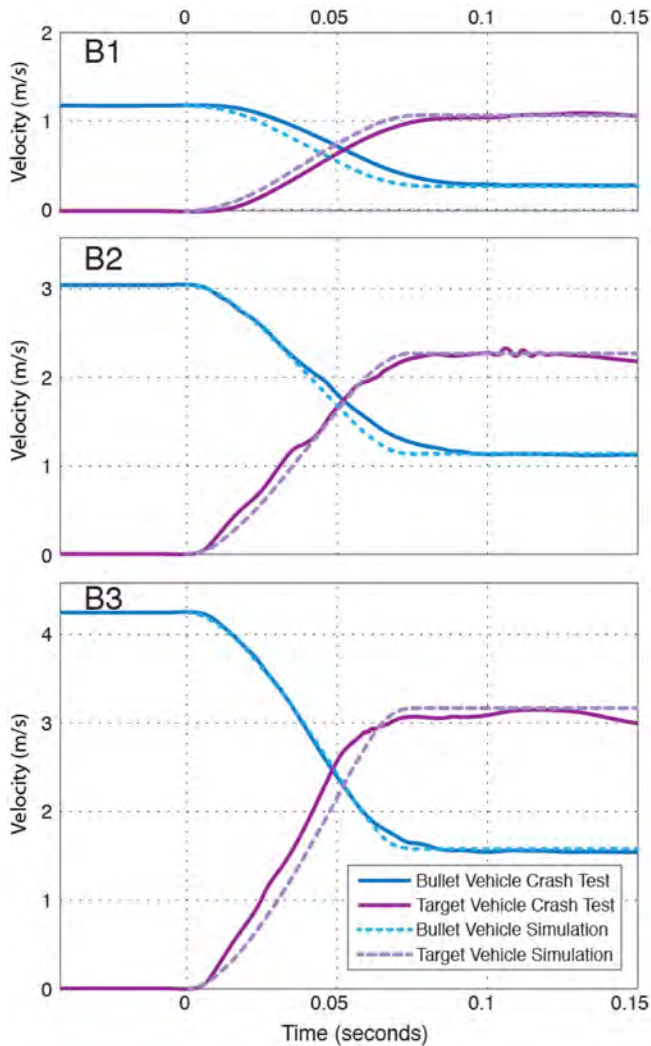


Figure 24. The velocities calculated in the simulations of Crash Tests B1, B2 and B3.

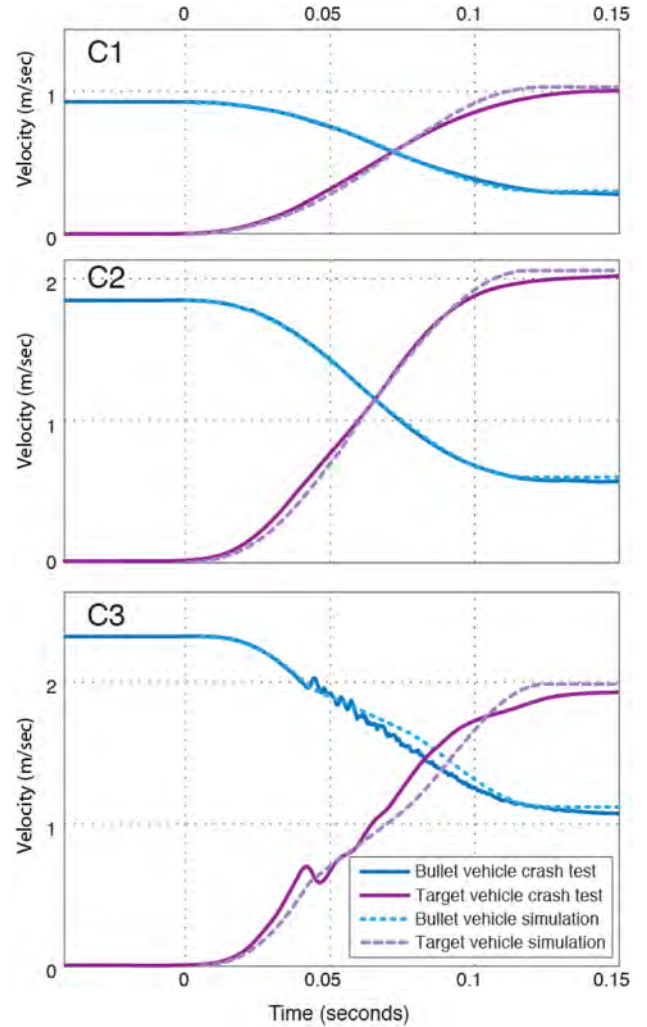


Figure 25. The velocities calculated in the simulations of Crash Tests C1, C2 and C3.

## DISCUSSION

An underlying assumption of the simulation model is that the QS F-D compression characteristics can be used to represent the dynamic F-D compression characteristics of a bumper system and this implies that there is no significant rate-dependent (viscoelastic) behavior of the bumpers as they are crushed. In the QS tests the bumper systems were crushed at a rate of 1.3 cm/s (0.5 in./s). In the crash tests the initial rate of deformation was the impact speed of the bullet vehicle, which had a range of 0.9 to 4.2 m/s (3.0 to 13.8 ft/s), and the rate of deformation decreased during the compression phase until it reached zero at maximum deformation. The QS and the dynamic F-D data were compared in Figures 20, 21, 22. The similarity between the compression phase of the QS and the dynamic F-D curves indicates that there was very little viscoelastic behavior of the bumpers during the compression phase of each crash in this study.

The impact bars in the 1994 Tercel rear bumper, the 2007 Ford Escape front bumper and the 2002 Honda Civic rear bumper and the face bar on the 2003 Chevy Express Van front bumper were made of steel. The impact bar in the 2008 Honda Civic rear bumper was aluminum and the impact bar in the 2005 Kia Sedona front bumper was glass mat thermoplastic (GMT). All of the bumpers had full covers made of thin polypropylene (PP), except the Chevy Express Van which only had the top 5 cm (2in.) of the face bar covered. Both Civics' bumpers and the Sedona's bumper had thin EPP impact absorbers between the impact bar and the bumper cover. The EPP does exhibit rate dependent behavior but it was not evident in this study, most likely because the EPP impact absorbers on the bumpers in this study were relatively thin. Bumpers with thicker EPP impact absorbers may exhibit significant viscoelastic behavior and the QS F-D characteristics may not accurately represent the dynamic F-D characteristics. Bumpers with plastic impact bars (for example, polypropylene impact bars) were not evaluated in this study and this type of impact bar may exhibit viscoelastic behavior, thus care should be taken in using this reconstruction technique in low-speed crashes that involve bumpers with plastic impact bars. Bumpers with piston-type energy absorbers have rate-dependent F-D characteristics in the deformation range where the piston strokes and the QS F-D characteristics cannot represent the dynamic characteristics in this deformation range.

A second assumption in the calculation of the vehicle velocities with the simulation model is that the vehicles are rigid bodies. The similarity between the velocities calculated with the simulation model and the measured crash test velocities (Figures 23, 24, 25) indicates that this assumption is valid in calculating the overall vehicle dynamics in the crash tests, but it is important to point out that the rigid body assumption also applies to the calculation of the vehicle velocities in the crash tests (Eqs. 4 and 5). There was evidence in the crash test data that indicates that the vehicles, especially the target vehicles, behaved as lumped masses during the crashes. In the graphs of the impact forces calculated with the load cell and the accelerometer data, Figures 17, 18, 19, the accelerometer-based impact forces ( $IF_T(t)$  and  $IF_B(t)$ , Eqs. 2 and 3) were higher than the load cell-based impact forces ( $IF_{LC}(t)$ ) during the first part of a crash, and lower than  $IF_{LC}(t)$  during the rebound phase of a crash. These differences between the accelerometer-based forces and the load cell-based forces were most pronounced for the target vehicles, which were production vehicles. The accelerometers on the target vehicle were attached to the body. The buck did not have a body, drive shaft, engine and transmission, although it did have a suspension and tires/wheels and the accelerometers were mounted directly to the frame.

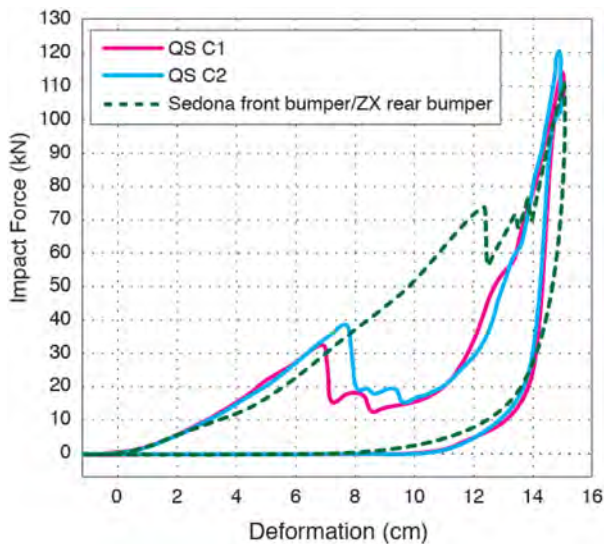
The differences between  $IF_T(t)$  and  $IF_{LC}(t)$  are thought to have occurred because of the movement of the target vehicle's body relative to its suspension, tires/wheels, engine/

transmission and drive shafts. During approximately the first 40 ms of the compression phase of a crash, the body moved forward relative to the true center of gravity (CG) of the target vehicle as the sprung mass was compressed. The accelerometers on the body indicated a higher acceleration than what was occurring at the true CG. Later on in the crash the sprung mass rebounded and the vehicle body moved rearward relative to the CG, and the accelerometers indicated a lower acceleration than what was occurring at the CG. The load cell impact force,  $IF_{LC}(t)$  (Eq. 1), is the net force acting on the vehicle if tire forces are neglected and a measure of the force acting on the vehicle's CG. Therefore,  $IF_T(t)$  was higher than  $IF_{LC}(t)$  early in a crash and lower than  $IF_{LC}(t)$  later in a crash. The same differences were seen between  $IF_{LC}(t)$  and  $IF_B(t)$ , but to a much smaller degree.

The effect of this sprung mass on the 2008 Honda Civic was very apparent in the target vehicle velocities for Crash Test C3 when the impact bar for the Sedona fractured (Figure 16). When the impact bar fractured at about 40 ms the acceleration of the Civic became negative and  $IF_T(t)$  became negative (Figure 19). This is a physical impossibility as there could be no impact force created at the bumpers that could grab the Civic and pull it back toward the buck during the crash. This negative acceleration measured the movement of the Civic's body, not the Civic's CG. The rapid reduction in the impact force when the Sedona's impact bar fractured allowed the force created in the sprung mass to push the Civic's body rearward relative to earth which resulted in the accelerometers on the body measuring a negative acceleration, the Civic's CG still kept accelerating forward. The same thing happened to  $IF_B(t)$ , which went from a negative to a positive force when the Sedona's impact bar fractured (Note that Figure 19 shows the absolute value of  $IF_B(t)$ ). When the Sedona's impact bar fractured,  $IF_{LC}(t)$  decreased from about 40 kN to 7 kN (8,992 to 1,574 lbs), but never became negative. Since the vehicle's accelerometer data were used to calculate the vehicle's velocities for the crash tests (Eqs. 4 and 5), these measured acceleration changes are reflected in the velocities in Figures 16 and 25 for Crash Test C3 where, at about 40 ms, the velocity of the Civic decreased and the velocity of the buck increased slightly. The velocities of the vehicles calculated in the simulation of Crash Test C3 do not show these changes at 40 ms because the model treats the vehicles as rigid bodies, and the impact force in the simulation of Crash Test C3 (dashed line in Figure 12) never becomes negative.

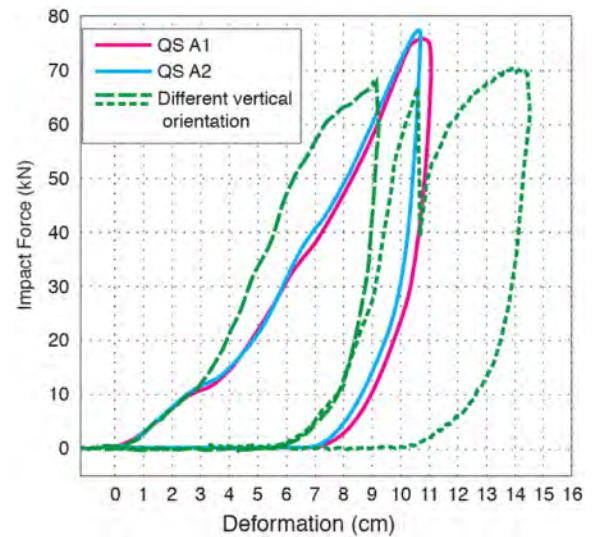
One of the unique features of the simulation model is that it treats the two bumpers that impact in a crash as a single entity, a bumper system. For a particular reconstruction the bumper system has two components; bumpers that are identical to those on the crash vehicles and an orientation similar to the bumpers in the crash. A change in one of the bumpers of the bumper system or a change in the orientation of the bumpers will affect the QS F-D curve.

Figure 26 shows the difference in the performance of the Sedona's front bumper in a QS F-D measurement when the 2008 Honda Civic rear bumper (Bumper System C) is replaced with a 1991 Nissan ZX rear bumper. The impact bar of the Nissan ZX's rear bumper and the Sedona's front bumper were aligned similar to Bumper System C for the measurement of the QS F-D curve shown in Figure 26. The Sedona's front impact bar fractured at a force of approximately 74 kN (16,635 lbs) with the Nissan ZX's bumper and at a force of 33 kN (7418 lbs) and 38 kN (8542 lbs) with the Civic's bumper (see Figure 12). The main reason for this difference in the fracture force appears to be that the Nissan's impact bar is flat and the Civic's impact bar is convex. The convexity in the Civic's impact bar placed greater loads at the contact point, which caused the Sedona's impact bar to fail at a lower overall compression force. Prior to the Sedona's impact bar fracturing, the F-D characteristics of both bumper systems were similar.



**Figure 26. Comparison of the QS F-D characteristics of two bumper systems that use the 2005 Kia Sedona's front bumper.**

Figure 27 shows the effect of a vertical orientation change on the QS F-D characteristics of Bumper System A. The face bar on the Chevy Express Van has a height of approximately 24 cm (9.4 in.) and in Bumper System A the top of the Tercel's bumper cover support brackets were approximately 6 cm (2.4 in) from the top of the face bar (see Figures 2 and 3). The van's face bar was raised approximately 8 cm (3 in.) relative to the Tercel's impact bar to create a new bumper system. The QS F-D measurement for this new bumper system is shown in Figure 27 along with QS A1 and QS A2. There were two separate measurements made with this new bumper system. The first measurement was stopped at a maximum deformation of 9.1 cm (3.6 in.) and the second measurement was stopped at a maximum deformation of 14.6 cm (5.7 in.).



**Figure 27. Comparison of the QS F-D characteristics of Bumper System A with another bumper system with the same bumpers but with the Express Van's face bar raised 7.6 cm (3 in.) higher than in Bumper System A.**

The different relative vertical position of the two bumpers resulted in a QS F-D curve that was different from QS A1 and QS A2 and different damage patterns to the bumpers. These differences occurred because there was less bending of the van's mounting brackets and more bending of the Tercel's mounting brackets. The drop in force in the second QS F-D curve of the new system at 10.5 cm (4.2 in.) occurred when the left mounting bracket of the Tercel broke away from its attachment hardware. After 14.5 cm (5.7 in.) of deformation the van's face bar had been crushed rearward but had not rotated like it did in the QS A1 and QS A2 measurements (see Figure 9). The Tercel's impact bar was forced upward as there was now significant deformation of the mounting brackets. In the measurement of QS A1 and QS A2 there was no significant deformation of the Tercel's mounting brackets. Thus, changing the vertical orientation of the bumpers in Bumper System A changed the QS F-D curve and the damage pattern to the bumpers. In a crash investigation therefore, it is important that the bumpers in the system have the same orientation as the bumpers in the crash being investigated. This will ensure that the damage patterns created to the bumpers in the QS F-D measurement are similar to the damage patterns of the bumpers on the crash vehicles. It will also ensure that the reconstructionist obtains the proper QS F-D data for use in the simulation model.

In the simulation of a crash test in this study the impact speed of the bullet vehicle and the coefficient of restitution for the crash test were known. In a real world investigation, the reconstructionist will not have this information. In order to use the simulation model the reconstructionist will need information on the damage to the bumpers in the crash being investigated. The bumper damage on the crash vehicles provides information on the orientation of the bumpers in the

crash and a metric to determine the maximum deformation in the simulation. In [Figure 10](#), the graphs of QS B1<sub>1</sub> and QS B1<sub>2</sub> demonstrated that the QS F-D measurement can be stopped to look at the bumper damage and then continued without affecting the overall QS F-D curve. By stopping the QS measurement, the reconstructionist can check the bumper system during a QS F-D measurement and compare the permanent damage of the test bumpers to the permanent damage to the bumpers of the crash vehicles. When the permanent damage to the bumpers in the QS F-D measurement equals or exceeds the permanent damage to the bumpers of the crash vehicles, that maximum deformation can be used in the simulation to determine the end of the compression phase of the crash. To do this the reconstructionist would iterate the impact speed of the bullet vehicle in the simulation until the target and bullet vehicles reached a common velocity at the selected maximum deformation. Therefore, the damage to the bumpers of the vehicles in the crash being investigated provides the information to determine when the crushing phase of that crash ends in the simulation.

Once the common velocity is reached in the simulation the reconstructionist must decide how to create the rebound IF-D curve in order to continue the simulation. There are two methods to do this. The first method requires the reconstructionist to select a coefficient of restitution ( $\epsilon$ ) and to determine a rebound IF-D curve that satisfies [Eqs. 9](#) and [10](#). For the simulations in this study, a straight line was used for the rebound IF-D. [Figure 28](#) shows the rebound curve used in the simulation of Crash Test A2 that was calculated in this manner, except the coefficient of restitution of 0.54 was known from the crash test data, and did not need to be estimated.

The second method is based on the similarity in the shape of the rebound curves of the QS and dynamic FD curves at a given force ([Figures 20, 21, 22](#)). In this method the rebound IF-D curve is created by placing the QS rebound curve on the point of maximum deformation in the simulation. The dark thick line in [Figure 28](#) that goes from (6.9 cm, 38.7 kN) to (3.5 cm, 0 kN) was created by moving the rebound portion of QS A2 to the left approximately 3.2 cm (1.3 in.). This approach imposes a coefficient of restitution on the simulated crash. The similarity between the two simulation rebound curves in [Figure 28](#) indicates that this is a reasonable approach. The coefficient of restitution that results from this approach in Crash Test A2 is 0.61, which is 13% higher than the 0.54 coefficient of restitution that was measured in that crash test.

This study demonstrated that the QS F-D data could be used in a simulation model to recreate the velocities of vehicles in a low-speed crash. If a reconstructionist is only interested in the  $\Delta V$ s of the vehicle, the QS F-D data can be used to provide the energy absorbed by both vehicles in the MER method ([7,8,9](#)). The similarity between  $E_{afc}$  and  $E_{afcm}$  in [Table 4](#) indicates that most of the energy absorbed in these

low-speed impacts was crush damage to the bumper system. The energy absorbed at a given amount of deformation can be obtained by integrating the QS F-D curve from zero deformation up to the chosen maximum deformation. Since the bumper system is composed of both bumpers, this integration is the energy absorbed by both vehicles minus the energy returned to the vehicles in the rebound phase of the crash, which is accounted for by the coefficient of restitution. An advantage of using the QS F-D with the MER method is the damage on the bumpers in the QS F-D measurement can be compared to the damage on the bumpers involved in the crash being investigated as a metric of how accurate the  $\Delta V$  estimates are. This technique can be used as long as the bumpers do not have any significant rate-dependent behavior.

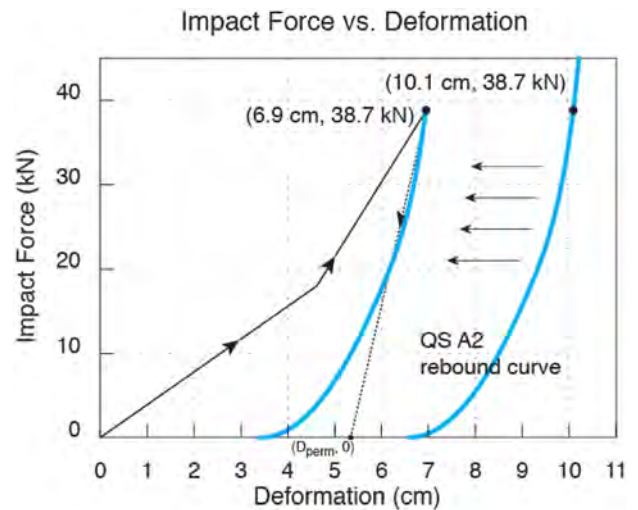


**Figure 28.** The rebound IF-D curve used in the simulation of Crash Test A2 is shown using a straight line approximation (dotted line) and based on the rebound part of the QS F-D curve.

The QS F-D data used in the low-speed simulation model has no relationship with the A and B coefficients in the CRASH3 algorithm ([11, 12](#)). These A and B coefficients represent the stiffness of one side of a single vehicle and can be used across a wide range of crash events that involve that side of the vehicle. The QS F-D data represent the stiffness of a bumper system that is made up of the bumpers from two different vehicles and these data are unique to the crash event being investigated because of the orientation requirement on the bumper system. The A and B coefficients are obtained from high speed barrier impacts where the damage is relatively uniform and many centimeters in depth. The QS F-D data are used to analyze crashes with low closing velocities where the resulting permanent damage is difficult to quantify with numerical values because it is usually not uniform in the vertical and lateral planes and the depth of the damage is minimal.

## SUMMARY/CONCLUSIONS

This study described a crash reconstruction technique that can be used to quantify the vehicle dynamics in low-speed bumper-to-bumper crashes where there is knowledge of damage to the bumpers on the vehicles involved in the crash. This reconstruction technique requires the measurement of the QS F-D characteristics of the bumpers involved in the crash. When this QS F-D data is input into the low-speed bumper-to-bumper simulation model (1) information on the velocities, accelerations and  $\Delta V$ s of the vehicles involved in the crash can be obtained. A comparison of the damage created in the measurement of the QS F-D characteristics with the damage created to the bumpers in the real world crash provides a metric to match the damage in the simulation with the damage to bumpers in the crash being investigated. This reconstruction technique was validated by recreating vehicle dynamics in crash tests using the QS F-D characteristics of the bumpers involved in the crash tests.

## ACKNOWLEDGMENTS

The authors acknowledge the work of Mr. John Martini who prepared the numerous graphs, tables and photographs that are presented in this manuscript.

The authors would also like to thank the reviewers for giving up their time to review this lengthy manuscript. Their comments and suggestions were helpful and appreciated.

## REFERENCES

1. Scott, W., Bain, C., Manoogian, S., Cormier, J. et al., "Simulation Model for Low-Speed Bumper-to-Bumper Crashes," *SAE Int. J. Passeng. Cars - Mech. Syst.* 3(1):21-36, 2010, doi: [10.4271/2010-01-0051](https://doi.org/10.4271/2010-01-0051).
2. Campbell, K., "Energy Basis for Collision Severity," SAE Technical Paper 740565, 1974, doi: [10.4271/740565](https://doi.org/10.4271/740565).
3. Thomson, R.W. and Romilly, D.P. "Simulation of Bumpers During Low Speed Impacts", Proceeding of the Canadian Multidisciplinary Road Safety Conference III. Saskatoon, Saskatchewan, Canada, 1993.
4. Ojalvo, I. and Cohen, E., "An Efficient Model for Low Speed Impact of Vehicles," SAE Technical Paper 970779, 1997, doi: [10.4271/970779](https://doi.org/10.4271/970779).
5. Ojalvo, I., Weber, B., Evensen, D., Szabo, T. et al., "Low Speed Car Impacts with Different Bumper Systems: Correlation of Analytical Model with Tests," SAE Technical Paper 980365, 1998, doi: [10.4271/980365](https://doi.org/10.4271/980365).
6. Brach, R., "Modeling of Low-Speed, Front-to-Rear Vehicle Impacts," SAE Technical Paper 2003-01-0491, 2003, doi: [10.4271/2003-01-0491](https://doi.org/10.4271/2003-01-0491).
7. Bailey, M., Wong, B., and Lawrence, J., "Data and Methods for Estimating the Severity of Minor Impacts," SAE Technical Paper 950352, 1995, doi: [10.4271/950352](https://doi.org/10.4271/950352).
8. Cipriani, A., Bayan, F., Woodhouse, M., Cornetto, A. et al., "Low Speed Collinear Impact Severity: A Comparison Between Full Scale Testing and Analytical Prediction Tools with Restitution Analysis," SAE Technical Paper 2002-01-0540, 2002, doi: [10.4271/2002-01-0540](https://doi.org/10.4271/2002-01-0540).
9. Happer, A., Hughes, M., Peck, M., and Boehme, S., "Practical Analysis Methodology for Low Speed Vehicle Collisions Involving Vehicles with Modern Bumper Systems," SAE Technical Paper 2003-01-0492, 2003, doi: [10.4271/2003-01-0492](https://doi.org/10.4271/2003-01-0492).
10. Collins, J.C. "Accident Reconstruction", Charles C. Thomas, Springfield, Illinois, USA, 1979.
11. McHenry, R.R. "Mathematical Reconstruction of Highway Accidents", DOT HS 801-405; Calspan Document No. ZQ-5341-V2, Washington, DC, 1975.
12. Noga, T. and Oppenheim, T.. "Crash3 User's Guide and Technical Manual," U.S. Dept. of Transportation, 1981.

## CONTACT INFORMATION

William R. "Mike" Scott  
Biodynamic Research Corporation  
5711 University Heights Blvd., Suite 100  
San Antonio, Texas 78249  
Phone: (210) 691-0281  
Fax: (210) 691-8823  
[mScott@brconline.com](mailto:mScott@brconline.com)